Segmentation Method for Bending Tools – Fundamental Investigation of Profile Forming by Segmented Tools

Jonas Reuter(✉), Peter Frohn-Sörensen, and Bernd Engel

Chair of Forming Technology, University of Siegen, Siegen, Germany
jonas.reuter@uni-siegen.de

Abstract. In bending processes with generic tools (e.g., three-roll push bending), the part geometry is a result of the free tool kinematics. In contrast, processes with geometry-specific tools (e.g., rotary draw bending) require a specialized tool geometry to form a dedicated part geometry. To make them more flexible while maintaining their advantages of dimensional accuracy and process controllability, adjustable tools are needed. Inspired by multi forming techniques, one possible approach is to segment the conventionally closed tool surfaces and adjust them in-process. For the design of the segmentation in terms of segment geometry and size, as well as in terms of tolerable spaces, a deep understanding of the deformation mechanisms of the workpiece in contact with segmented surfaces is crucial. As a first step toward this goal, this work presents lateral indentation tests of circular and square steel and aluminum tubes by segments and segmented surfaces. Based on these tests, finite element (FE) models are validated and show a good correlation with the experimental tests in terms of force-displacement curves and part geometries. Finally, the FE-model is used to perform a parameter study to investigate the deformation behavior of tubes subjected to lateral loading by segmented surfaces in dependency of different tube wall thicknesses as well as of different segment spacings. It is outlined, that the segmentation of forming tools is generally possible with negligible impact on the process when choosing a suitable surface topology.

Keywords: Profile Bending · Profile Forming · Adjustable Forming Tools · Segmented Forming Tools · Forming Flexibility · DIC

1 Introduction

Increasing mass customization and product individualization require agile, flexible, and smart production systems in manufacturing technology [1]. Forming processes with generic tools own an inherent flexibility due to their free tool movement (e.g., single point incremental forming [2], three-roll push bending [3]). In contrast, processes with geometry-specific tools or shape-related tools (e.g., rotary draw bending [4]) are limited in the variety of part geometries that can be manufactured with a single tool set. However, latter offer advantages in terms of dimensional accuracy, process controllability and the

K. Mocellin et al. (Eds.): ICTP 2023, LNME, pp. 547–559, 2024.
https://doi.org/10.1007/978-3-031-41023-9_55

ability to form strong curvatures. To maintain these advantages while becoming more flexible, adjustable tools are needed. Small contour changes, e.g. to control the local material flow by an adaptive blank holder in deep drawing, can be generated by elastic adjustments [5]. For large contour changes of the forming die surfaces, their geometrical break-up is crucial. For this purpose, a method for the design of reduced bending tools with additional tool axes is presented in [6], which is based on the numerical analysis of the contact pressure distribution of conventional processes with closed surfaces.

State of The Art: Multi-Point Forming and Part Defects. Also, multi-point forming (MPF) or digitized-die forming (DDF) techniques respectively with discrete, reconfigurable tools basically offer a way to make shape-related processes more flexible. In the field of sheet metal forming, several authors investigate the design and algorithms for the shape generation of reconfigurable dies for stretch-forming of large-scale parts [7–10]. Li et al. [11, 12] present a MPF process with an upper and a lower die, each consisting of many punches. They study the sectional forming, emphasize the advantage of in-process variation of the forming path and develop a closed-loop control for spring-back compensation. However, the local, inhomogeneous punch contacts can lead to part defects. The main ones identified by numerous authors are surface dimples, wrinkles and local shape deviations [11–17]. Intermediate layers between tool and workpiece of polyurethane [11–15, 17], for instance, or pivotable, flat punch heads [16] are used to contain these defects. Nevertheless, the basic tool and process parameters are essentially responsible for the occurrence of defects, with the following interrelationships being known: From numerical and experimental tests based on statistical experimental design as well as a statistical evaluation, it is known that punch size and punch head radius have a significant influence on wrinkles, sheet thickness variation and shape deviation [14]. According to [17], the higher the punch density and punch size, the lower the occurrence of dimples and local shape deviations. The punch head geometry itself is of secondary importance, as shown by comparing hemispherical and saddle-shaped punch heads with otherwise comparable area dimensions of the punches [18]. Similar findings to those for MPF in sheet metal forming can also be found in profile forming. Here, an additional component defect is the cross-sectional deformation. In multi-point stretch bending of open aluminum profiles with large bending radii, the shape deviation can be reduced by increasing the number of die segments [19]. The cross-sectional deformation of rectangular aluminum profiles increases with increasing bending angle during multi-point stretch bending, see [20]. Applying the MPF to the die bending of extruded closed aluminum profiles, [21] find that dimpling decreases with increasing die punch size as well as with the use of an intermediate layer of spring steel. Furthermore, they find that by varying the forming path, the cross-sectional deformation can be influenced, and thus smaller bending radii be realized.

State of the Art: Tube Deformation in Lateral Indentation. A review of the literature reveals that there are basic studies on the deformation behavior of tubes subjected to local lateral loads. Fundamental experimental series on the lateral indentation of round tubes by means of a wedge-shaped punch have been performed by [22–24]. They phenomenologically describe the deformation behavior as a function of the ratios of tube length and diameter to wall thickness for both, unilateral indentation under a three-point bending load and bilateral indentation by opposing punches. Further studies [25]

develop mechanical models describing the load-deflection curve and the geometry of the deformed zone under various combined boundary conditions of the tube. They conclude the essential finding that the resistance of the tube cross-section significantly depends on the boundary conditions of the tube. This is further confirmed by several research [26–28] investigating the influence of an internal pressure and of a compliant embedment on the load-deformation behavior. The higher the pressure the greater the indentation resistance and the smaller the plastically deformed zone. The shape of the indentor plays a subordinate role, as comparisons between wedge-shaped and spherical ones show. In contrast, the compliance of the embedment and the embedment depth have a significant influence. In addition, a parametric study was conducted by [29] using FE simulations to investigate the influence of wall thickness, pipe length, and yield stress on the load-deformation behavior of flat supported circular pipes under a discrete radial load. The numerical calculations show good agreement with the analytical model of [25]. Furthermore, based on the analytical model of [30], an analytical model has been developed by [31] to describe the radial indentation of hemispherical tool elements during incremental profile forming. The model describes the wall thickness reduction in the contact zone and the process force as a function of the indentation depth, accounting for the tool and workpiece geometry as well as mechanical material properties. It is highlighted that the plastically deformed zone can be divided into a small, shape-bound contact area and a significantly larger, free forming zone.

Objective, Scope and Procedure. MPF is a flexible metal forming technology. Previous work has focused on process development for large-sized parts. Some contributions provide correlations between tool and process parameters and the resulting part geometry. However, to the best of the authors' knowledge, there is no systematic design method for such a discrete tool surface based on the deformation mechanisms of the workpiece – especially not for profile bending with small radii. Therefore, as a first step towards the development of such a design method, fundamental experimental tests are carried out to characterize the load-deformation behavior of tubes subjected to lateral loads by segments and segmented surfaces. These results are used to validate finite element (FE) models. Finally, a simulation-based phenomenological parameter study provides insight into the relationship between geometric surface parameters, workpiece properties and tube deformation behavior.

2 Experimental Investigations

Extruded aluminum tubes (material AlMgSi0.5 F22; EN AW-6060 T66) and roll-formed as well as cold-drawn steel tubes (material E235 +C/+N) with circular and square cross sections, with outer dimensions of 30 mm and nominal sheet thicknesses of 1.5 mm, 2.0 mm and 3.0 mm are available as test materials.

2.1 Mechanical Characterization

To conduct tensile tests according to DIN EN ISO 6892-1, dumbbell shaped specimens with a width of 12.5 mm and a parallel length of 75 mm were taken from the square

tubes by milling. The circular tubes were cut to a length 300 mm. Solid mild steel inner mandrels at the tube ends allow for hydraulic clamping.

Testing was performed on a ZWICK ROELL Z250 universal testing machine with a constant feed rate of 0.04 mm/s with 3 to 5 repetitions per series. Digital Image Correlation (DIC) was utilized using a GOM ARAMIS 12M system to determine the longitudinal elongation within the 50 mm gauge length and transverse strain for r-value calculation. The system was calibrated for a field of view of 200 × 147 mm^2 resulting in a local resolution of 20.5 pixel/mm. The force signal of the testing machine was coupled with the DIC system via 0–10 V DC analog interface. Table 1 shows the mechanical properties.

Table 1. Mechanical properties of the test material determined in uniaxial tensile tests.

Material	Specimen geometry	Nominal thickness [mm]	Ag [%]	R_{eL} or $R_{p0,2}$ [MPa]	Rm [MPa]	r_0-value [–]
E235 +C	Tube	1.5	6.3 ± 0.2	442.8 ± 7.1	476.0 ± 7.1	0.80 ± 0.02
E235 +N	Tube	2.0	22.8 ± 0.1	287.2 ± 7.6	407.6 ± 8.1	1.10 ± 0.01
E235 +N	Tube	3.0	19.3 ± 0.3	279.3 ± 2.2	410.7 ± 2.2	1.03 ± 0.02
E235 +N	Dumbbell	1.5	12.4 ± 1.2	456.6 ± 10.7	478.5 ± 9.7	0.83 ± 0.02
E235 +N	Dumbbell	2.0	6.8 ± 0.5	446.7 ± 4.5	488.0 ± 4.4	0.90 ± 0.01
E235 +N	Dumbbell	3.0	2.0 ± 0.4	381.0 ± 7.4	389.7 ± 9.6	0.80 ± 0.04
AW-6060	Tube	1.5	8.6 ± 0.1	206.1 ± 2.9	240.4 ± 2.7	0.49 ± 0.01
AW-6060	Tube	2.0	9.5 ± 0.3	245.6 ± 1.8	277.8 ± 7.1	0.60 ± 0.01
AW-6060	Tube	3.0	6.7 ± 0.0	249.0 ± 0.4	266.3 ± 0.3	0.60 ± 0.01
AW-6060	Dumbbell	2.0	7.1 ± 0.2	206.9 ± 1.8	230.4 ± 1.8	0.45 ± 0.02
AW-6060	Dumbbell	3.0	10.9 ± 0.1	210.1 ± 0.4	248.8 ± 0.3	0.45 ± 0.05

2.2 Lateral Indentation Tests

To validate FE models that sufficiently capture the load-deformation behavior, lateral indentation tests were performed on the universal testing machine ZWICK ROELL Z250. Figure 1 shows the test setup. Different segment geometries, namely straight segments with radii of R = 1|2|5 mm and circular segments, can be placed at various positions in fixture. The segment spacing a = 20|30|40 mm can be varied by the changing the mounting. Small HBM C9C load cells measure the force of each segment. A GOM ARAMIS 12M DIC system with the settings described above is used to measure local tool displacement due to the applicated reference points as well as surface strains of the specimens.

Figure 2a shows the force displacement curves of lateral indentation tests with a single segment, while Fig. 2b show those with three segments with a space of a =

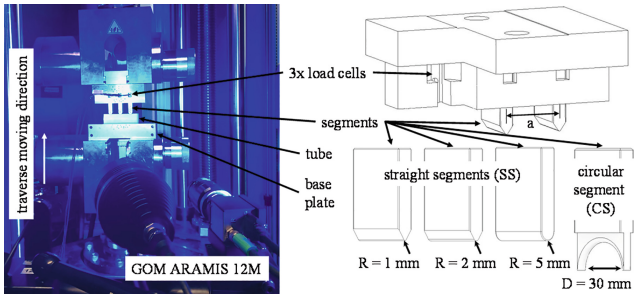

Fig. 1. Test setup for the lateral indentation tests.

30 mm and opposing flat plates, representing a conventionally closed tool surface as reference.

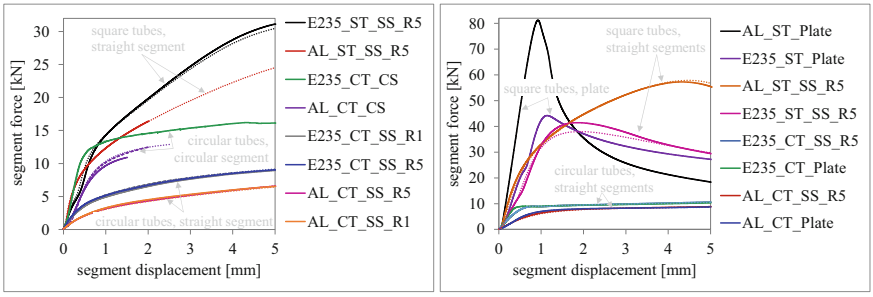

(a) indentation tests with 1 segment

(b) indentation tests with three segments with a spacing of a = 30 mm and plates

Fig. 2. Force-displacement curves of lateral indentation tests using steel and aluminum tubes with circular and square cross sections with a nominal thickness of 2.0 mm, outer dimensions of 30 mm and a length of 100 mm. Nomenclature: E235 – steel of grade E235; AL – aluminum of grade AW-6060; ST – square tube; CT – circular tube; SS - straight segment; Rx – segment radius of x mm; CS – circular segment.

In Fig. 2a, it can be seen that lateral indentation tests of circular tubes (CT) with one circular segment (CS) have a significantly different load deformation characteristic than with a single straight segment (SS). During indentation with SS, there is a smooth transition from the linear elastic to the plastic region. In contrast, the CS indentations show a more distinct transition. In addition, the linear slopes and the forces in general are much higher due to the increased contact area of the enveloping line contact compared to the point contact of the SS. Comparing aluminum (AL) to steel (E235) tubes, with otherwise the same test parameters, lower linear slopes and forces are evident. This is due to the approximately three times lower Young's Modulus and a different strain hardening behavior. As reported by [18], the segment radius has a negligible effect on the load deformation behavior. It is interesting to note that the initial slope of the force-displacement curves for E235 is lower than that for AL in the case of the square tubes (ST). Responsible is the initial geometry, because the faces of the roll-formed E235 tubes

are slightly convex. Therefore, during the first few tenths of the segment displacement a local bending of the faces takes place until the full contact is reached.

The same effect can be seen for lateral indentation of square tubes with plates and three SS. In both cases, the initial slopes of the force-displacement curves and the maximum forces are higher for the AL tubes, see Fig. 2b. Again, the convex faces of the E235 tubes cause an early bulging. Against this, the straight faces of the AL tubes remain straight and therefore the increasing segment force is due to plastic deformation in the sheet thickness direction in the contact zone until a global cross section deformation occurs.

With regard to the long-term goal of the research, the development of a design method for segmented tool surfaces, it is worth to mention that the indentation of circular tubes with plates and three segments show very similar load deformation behavior, except for slight differences in the transition from linear elastic to plastic deformation caused by local indentations of segments.

3 Validation of a Finite Element Model

The flow curves are approximated using the El-Magd [32], Ludwik [33] and Voce [34] approaches, see Table 2. The parameters were determined from test data described in Sect. 2.1 by curve fitting using the least-square method.

Table 2. Flow curve approximations used for the FE-simulations. The parameters were determined by least squares curve fitting of test data from tensile tests on circular tubes with a nominal thickness of t = 2.0 mm.

	El-Magd [32]	Ludwik [33]	Voce [34]
	$k_f(\varphi) = C_1 + C_2 \cdot \varphi + \ldots$ $\ldots C_3 \cdot (1 - e^{-\varphi/C_4})^n$ with $C_1 = 296.3$; $C_2 = 432.7$; $C_3 = 128.9$; $C_4 = 0.04$; $n = 2.4$	$k_f(\varphi) = k_{f0} + \ldots$ $\ldots A \cdot \varphi^n$ with $k_{f0} = 190.2$; $A = 118.1$; $n = 0.12$	$k_f(\varphi) = k_{fs} - \ldots$ $\ldots (k_{fs} - k_{f0}) e^{-m \cdot \varphi}$ with $k_{fs} = 327.8$; $k_{f0} = 243.7$; $m = 14.6$
E235	$0 < \varphi < 1.0$		
AL		$0 < \varphi < 0.015$	$0.015 \leq \varphi < 1.0$

HyperWorks 2022 was used for to design the FE-models for the LS- Dyna R12.0.0 solver. Selectively reduced, fully integrated hexahedral elements (ELFORM = −2 in *SECTION_SOLID) with a nominal element size of 0.5 mm in square and 0.4 mm in the thickness direction (5 elements over thickness) are used for the discretization of the tubes, see Fig. 3a. The tube wall thickness of the circular tubes is modeled as measured for each test material with a conventional micrometer. To better account for local contact pressure distribution, the forming segments are discretized with solid elements as well, namely constant stress tetrahedrons (ELFORM = 13) with a nominal element size of

0.15 mm in the contact area and 2 mm elsewhere. The base plate is modeled with rigid shells. To account for real tool geometries, relevant dimensions were measured and transferred to the FE model.

The *CONTACT_FORMING_ONE_WAY_SURFACE_TO_SURFACE card was selected for numerical contact modeling, wherein the static friction coefficient is set to 0.1. According to the test setup, a prescribed segment velocity is modeled using the *BOUNDARY_PRESCRIBED_MOTION card, which is linked to the master node of a *CONSTRAINED_NODAL_RIGID_BODY, and the reaction forces are evaluated. The linear elastic *MAT_001 is defined as segment material and the v. Mises isotropic elastic-plastic *MAT_024 as tube material.

Figure 3b shows the comparison of selected force-displacement curves from experimental tests and FE simulations. For the E235 tubes, a satisfying correlation between the calculated and the test curves is obtained. However, the simulation slightly overestimates the measured forces, except for the indentation tests with one straight segment, where there are no significant deviations. For the indentation of a single circular segment (top curve), the simulation shows an alternate behavior at a segment displacement of about 4 mm, which is a result of the numerical contact trying to prevent the sharp edges at the end of the semi-enclosing segment from penetrating into the tube wall. For the indentation of AL tubes (lower curves), the calculated curve differs significantly from the measured one. An obvious reason is the anisotropy of the AL, which is not implemented in the FE model until now. And, to smaller accounts, AL has a higher static coefficient of friction towards tool steel.

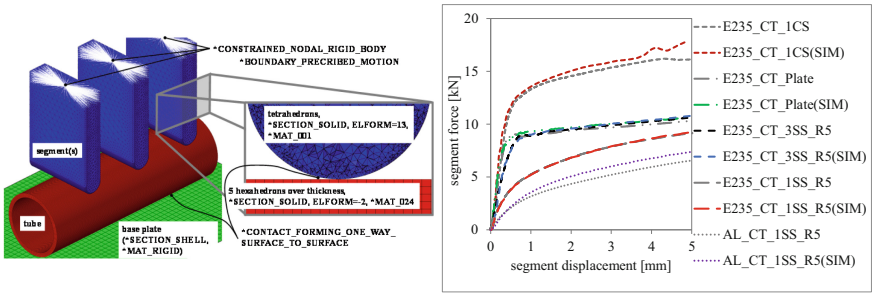

(a) FE-model setup

(b) Comparison of force-displacement curves from test and FE simulation

Fig. 3. FE-model setup and Comparison of force-displacement curves from test and FE-simulation.

The deformed specimens from the lateral indentation tests (see Fig. 2) were digitized using a GOM ATOS CORE scanner and the surface deviations between the test specimens and the simulation geometries were analyzed using the GOM INSPECT 2020 software. The very good correlation between the force-displacement curves from the tests and simulations is confirmed by the good correlation between the part geometries, as shown in Fig. 4 for three selected test cases. Here, the resulting surface deviations are maximum 0.17 mm, which corresponds to approximately 3% of the segment displacement.

In addition, the strain maps measured by DIC are generally in good agreement with the simulated ones with respect to the mustache-shaped strain distribution. However, the measured v. Mises strains are generally about 0.015 higher than the calculated strains (Fig. 5).

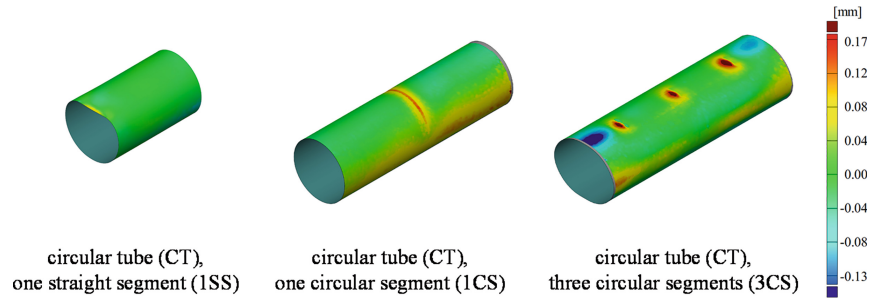

Fig. 4. Surface deviations between selected deformed E235 steel test specimens with a wall thickness of 2.0 mm from lateral indentation tests with segment strokes of 5 mm and the corresponding simulation after springback.

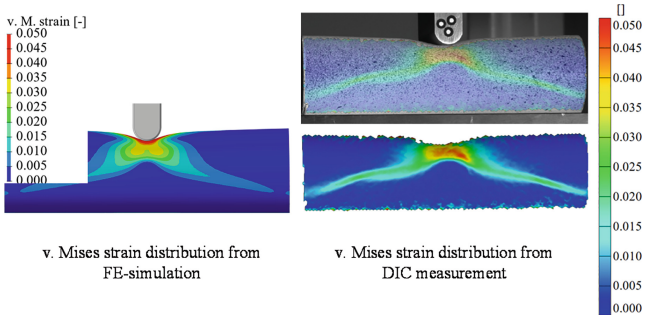

Fig. 5. Comparison of v. Mises strain distribution from FE-simulation (left) and DIC-measurement (right) of a lateral indentation of a circular E235 steel tube with a wall thickness of 2.0 mm and with an outer diameter of 30 mm by one straight segment with R = 5 mm radius.

4 Deformation Phenomena Due to Lateral Loading by Segmented Surfaces

The validated FE-models can be used for virtually investigating the deformation behavior of tubes subjected to lateral loading by segmented surfaces in a phenomenological comparison study. For this, a setup according to Fig. 3a is chosen with a circular tube with a diameter of 30 mm and a length of 130 mm. The number of segments and at the same time the space between the segments is varied from 11 to 3 segments or from a = 12 mm to a = 60 mm space respectively for the three wall thicknesses t = 1.0|2.0|3.0 mm.

The deformation behavior of a tube compressed by two flat plates, representing a conventionally closed tool surface, is used as reference for the comparison study. Figure 6 shows the segment force vs. segment displacement curves of the simulations performed. Trivially, the indenting resistance of the cross section increase with increasing wall thickness. Comparing the curves of the same wall thicknesses, it is evident that the load-deformation behavior approaches to the characteristic of the compression with plates as the number of segments increases. This effect is more pronounced for larger wall thicknesses. In geometric terms, this means that the cross-sectional deformation evolves from one dominated by local indentations to a more global cross-sectional deformation.

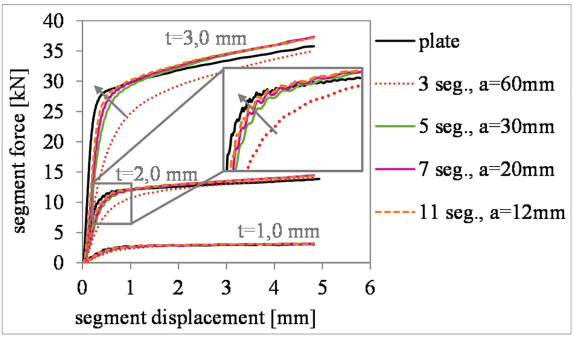

Fig. 6. Simulated load-deformation behavior of lateral indentation of circular E235 steel tubes with different wall thicknesses by flat plates, representing a conventionally closed tool surface, and by segmented surfaces.

This can also be seen in the longitudinal sections in the deformed state after lateral indentation (segment displacement of 5 mm), see Fig. 7.

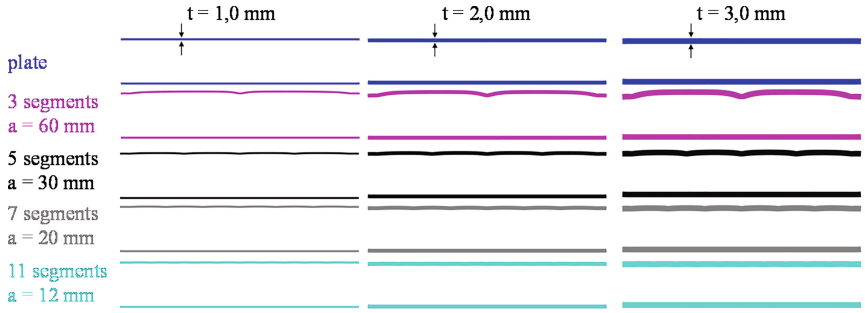

Fig. 7. Longitudinal sections out of FE-Simulation of circular E235 steel tubes after lateral indentation in the deformed state for different segmentations and different wall thicknesses.

For the lateral compression of the tubes by flat plates (first row), a continuous cross-sectional deformation over the tube length is observed. In contrast, the longitudinal sections after 3-segment lateral indentation (second row) show distinct local features.

These are reduced as the number of segments increases or the segment spacing decreases respectively, and a more global and continuous deformation over the tube length takes place. For smaller wall thicknesses, for a selected segmentation a more continuous deformation is observed compared to larger wall thicknesses due to of the reduced resistance of the cross section against cross-sectional deformation. Figure 8 shows the corresponding cross sections to the longitudinal sections of Fig. 7 indicating a ring mode deformation [23], where the same phenomena described before can be observed: For increasing segment number, the more the cross-sectional geometry resembles that obtained by the compression of two opposing flat plates.

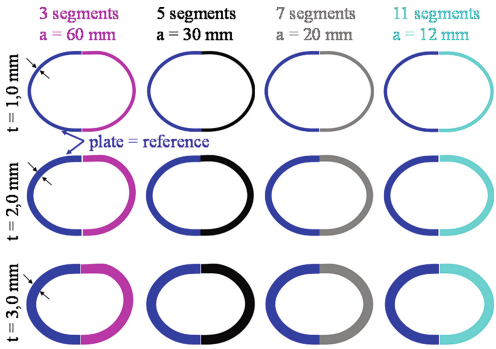

Fig. 8. Cross sections out of FE-simulation of circular E235 steel tubes after lateral indentation in the deformed state for different segmentations and different wall thicknesses.

5 Conclusion and Outlook

In this paper, we have presented an excerpt from our ongoing work on the development of a design method for segmented bending tool surfaces and the development of strategies for the in-situ adjustment of these segmented surfaces to increase manufacturing flexibility. We have described the lateral indentation tests performed for both, to characterize the plastic deformation behavior of circular and square tubes subjected to lateral loading by segments and segmented surfaces, and to validate finite element models. We plan to conduct further experimental tests with additional tube geometries specified in Table 1 using a design of experiment (DoE) approach.

The simulation results with the explicit solver LS-DYNA R12.0.0 are in good correlation with the experimental tests regarding the force-displacement curves and the geometries for circular E235 steel tubes with a wall thickness of 2.0 mm. With respect to the strain distribution, the overall shape of the strain map fits very well to the test-based strain map measured by DIC. However, there are deviations in terms of the strain values of about 0.015, which should be clarified in future work. For circular aluminum tubes the computed and the measured force-displacement curve exhibit considerable deviations. We assume, that the anisotropy of the aluminum alloy, which is not yet implemented in the FE-model, is responsible. Forthcoming work will focus on the determination of

the r-values their implementation in the FE-model. Finally, a parameter study was performed to investigate the deformation behavior of tubes subjected to lateral loading by segmented surfaces in dependency of different tube wall thicknesses as well as of different segment spacings. The resulting force-displacement curves in Fig. 6 together with the sectional geometries in Figs. 7 and 8 point out, that the plastic deformation behavior tends to approximate that of a tube compressed by two opposing flat plates, representing a conventionally closed tool surface. This phenomenon is crucial, because it indicates that a segmentation of forming tool surfaces will generally be possible with negligible impact on the process. To this end, a thorough understanding of the cause-effect relationships between the segmented tool geometry, the workpiece properties, the boundary conditions, the effective contact pressure distribution and the workpiece deformation is required and is part of the research project mentioned below. Especially, the influence of the bending stress, if considering tubes under bending loads instead straight tubes lying on a flat plate, is important since boundary conditions significantly influence the indenting resistance [25].

Acknowledgement. This research is part of a project funded by the Deutsche Forschungsgemeinschaft (DFG, German Research Foundation) – project number 509709804.

References

1. Yang, D.Y., et al.: Flexibility in metal forming. CIRP Ann. **67**, 743–765 (2018)
2. Duflou, J.R., et al.: Single point incremental forming: state-of-the-art and prospects. Int.J. Mater. Form. **11**(6), 743–773 (2017). https://doi.org/10.1007/s12289-017-1387-y
3. Ghiotti, A., Simonetto, E., Bruschi, S., Bariani, P.F.: Springback measurement in three roll push bending process of hollow structural sections. CIRP Ann. **66**, 289–292 (2017)
4. Borchmann, L., Schneider, D., Engel, B.: Design of a fuzzy controller to prevent wrinkling during rotary draw bending (2021). https://popups.uliege.be/esaform21. https://popups.uliege.be/esaform21/index.php?id=2742. Accessed 20 Feb 2023
5. Elend, L.-E.: Einsatz elastischer Niederhaltersysteme zur Erweiterung der Prozeßgrenzen beim Tiefziehen (2001). https://doi.org/10.15488/5808
6. Heftrich, C., Steinheimer, R., Engel, B.: Rotary-draw-bending using tools with reduced geometries. Procedia Manuf. **15**, 804–811 (2018)
7. Olsen, B.A.: Die Forming of Sheet Metal using Discrete Surfaces. Massachusetts Institute of Technology (1980)
8. Hardt, D.E., Webb, R.D., Suh, N.P.: Sheet metal die forming using closed-loop shape control. CIRP Ann. **31**, 165–169 (1982)
9. Walczyk, D.F., Lakshmikanthan, J., Kirk, D.R.: Development of a reconfigurable tool for forming aircraft body panels. J. Manuf. Syst. **17**, 287–296 (1998)
10. Walczyk, D.F., Hardt, D.E.: Design and analysis of reconfigurable discrete dies for sheet metal forming. J. Manuf. Syst. **17**, 436–454 (1998)
11. Li, M.Z., Cai, Z.Y., Sui, Z., Yan, Q.G.: Multi-point forming technology for sheet metal. J. Mater. Process. Technol. **129**, 333–338 (2002)
12. Li, M.-Z., Cai, Z.-Y., Liu, C.-G.: Flexible manufacturing of sheet metal parts based on digitized-die. Robot. Comput. Integr. Manuf. **23**, 107–115 (2007)
13. Cai, Z.-Y., Wang, S.-H., Li, M.-Z.: Numerical investigation of multi-point forming process for sheet metal: wrinkling, dimpling and springback. Int. J. Adv. Manuf. Technol. **37**, 927–936 (2008)

14. Abosaf, M., Essa, K., Alghawail, A., Tolipov, A., Su, S., Pham, D.: Optimisation of multi-point forming process parameters. Int. J. Adv. Manuf. Technol. **92**(5–8), 1849–1859 (2017). https://doi.org/10.1007/s00170-017-0155-y
15. Elghawail, A.M., et al.: Measurement of forces on multi-point forming tools using fibre Bragg grating sensors. Proc. Inst. Mech. Eng. Part B: J. Eng. Manuf. **234**, 453–462 (2020)
16. Selmi, N., BelHadjSalah, H.: Ability of the flexible hydroforming using segmented tool. Int. J. Adv. Manuf. Technol. **89**(5–8), 1431–1442 (2016). https://doi.org/10.1007/s00170-016-9160-9
17. Wang, S., Cai, Z., Li, M.: Numerical investigation of the influence of punch element in multi-point stretch forming process. Int. J. Adv. Manuf. Technol. **49**, 475–483 (2010)
18. Paunoiu, V., Cekan, P., Gavan, E., Nicoara, D.: Numerical simulations in reconfigurable multipoint forming. Int. J. Mater Form **1**, 181–184 (2008)
19. Lin, X., et al.: Effect of flexible 3D multipoint stretch bending dies on the shape accuracy and the optimal design. Adv. Mater. Sci. Eng. **2018**, e1095398 (2018)
20. Liang, J., Liao, Y., Li, Y., Liang, C.: Study on the influence of bending angle of multipoint stretch-bending of profiles on section distortion of parts. Math. Probl. Eng. **2020**, e1975805 (2020)
21. Liu, X.Z., Liu, C.G., Yao, Y., Zhang, X.G.: Numerical analysis for multi-point forming of aluminum alloy profile. Adv. Mater. Res. **1035**, 128–133 (2014)
22. Thomas, S.G., Reid, S.R., Johnson, W.: Large deformations of thin-walled circular tubes under transverse loading – I. An experimental survey of the bending of simply supported tubes under a central load. Int. J. Mech. Sci. **18**, 325–333 (1976)
23. Watson, A.R., Reid, S.R., Johnson, W., Thomas, S.G.: Large deformations of thin-walled circular tubes under transverse loading – II. Experimental study of the crushing of circular tubes by centrally applied opposed wedge-shaped indenters. Int. J. Mech. Sci. **18**, 387–397 (1976)
24. Watson, A.R., Reid, S.R., Johnson, W.: Large deformations of thin-walled circular tubes under transverse loading – III. Further experiments on the bending of simply supported tubes. Int. J. Mech. Sci. **18**, 501–502 (1976)
25. Wierzbicki, T., Suh, M.S.: Indentation of tubes under combined loading. Int. J. Mech. Sci. **30**, 229–248 (1988)
26. Karamanos, S.A., Andreadakis, K.P.: Denting of internally pressurized tubes under lateral loads. Int. J. Mech. Sci. **48**, 1080–1094 (2006)
27. Arabzadeh, H., Zeinoddini, M.: A closed-form solution for lateral indentation of pressurized pipes resting on a flexible bed. Int. J. Mech. Sci. **75**, 189–199 (2013)
28. Zeinoddini, M., Arabzadeh, H., Ezzati, M., Parke, G.A.R.: Response of submarine pipelines to impacts from dropped objects: bed flexibility effects. Int. J. Impact Eng. **62**, 129–141 (2013)
29. Brooker, D.C.: A numerical study on the lateral indentation of continuously supported tubes. J. Constr. Steel Res. **60**, 1177–1192 (2004)
30. Liu, J.H., Francis, A.: Theoretical analysis of local indentation on pressured pipes. Int. J. Press. Vessels Pip. **81**, 931–939 (2004)
31. Grzancic, G., Löbbe, C., Ben Khalifa, N., Tekkaya, A.E.: Analytical prediction of wall thickness reduction and forming forces during the radial indentation process in incremental profile forming. J. Mater. Process. Technol. **267**, 68–79 (2019)
32. El-Magd, E., Treppman, C., Korthäuer, M.: Description of flow curves over wide ranges of strain rate and temperature. Int. J. Mater. Res. **97**, 1453–1459 (2006)

33. Ludwik, P.: Elemente der Technologischen Mechanik (1909). https://doi.org/10.1007/978-3-662-40293-1
34. Voce, E.: The relationship between stress and strain for homogeneous deformation. J. Inst. Met. **74**, 537–562 (1948)